BER the international journal of bridge engineering management and research

Smart Acoustic Sounding for Automated Delamination Detection in Concrete Bridge Decks

Deepak Kumar[1,*]; Anil K. Agrawal[2]; and Ran Cao[3]

Submitted: 14 August 2025 **Accepted:** 15 September 2025 **Publication date:** 10 October 2025

DOI: 10.70465/ber.v2i4.54

Abstract: Concrete bridge decks are susceptible to subsurface defects such as delamination, caused by aging, corrosion, and environmental stressors, underscoring the need for timely, reliable nondestructive evaluation. While traditional acoustic methods, such as hammer or chain drag, remain widely used, they suffer from subjectivity, inconsistent impact forces, and limited applicability on overhead or vertical surfaces.

This study introduces a novel Smart Acoustic Sounding System that modernizes impact sounding through an integrated framework consisting of a broadband electronic chirp excitation source, high-sensitivity Micro-Electro-Mechanical Systems microphones with acoustic shielding, and a tracking camera for automated and location-aware inspections. Advanced signal processing techniques, such as empirical mode decomposition, power spectral density, and the Hilbert–Huang transform, are employed to filter noise, extract frequency-based features, and support machine learning–based defect classifications. Laboratory testing on a full-scale concrete slab embedded with known artificial defects (e.g., shallow and deep delamination, voids, and honeycombing), as well as a deteriorated concrete beam, confirmed the system's ability to accurately identify defect zones, particularly shallow delamination with characteristic frequency signatures in the range of 1–3 kHz. The system produced real-time defect maps with minimal human input, demonstrating its potential to improve the accuracy, repeatability, and efficiency of bridge deck inspections and support data-driven maintenance decisions.

Author keywords: Structural health monitoring; delamination detection; concrete bridge decks; acoustic impact sounding; machine learning; nondestructive evaluation; signal processing

Background and Motivation

Concrete structures, especially bridges, are critical components of transportation infrastructure. Their timely inspection and maintenance are essential to ensure public safety and uninterrupted service. In the United States, the American Society of Civil Engineers (ASCE) estimates that over 42,000 bridges (approximately 6.8%) are in poor condition, and nearly 45% have exceeded their original 50-year design life.[1] These statistics underscore the urgent need for scalable, accurate, and objective inspection methods to assess structural health, particularly for aging concrete bridge decks prone to subsurface deterioration. Among various deterioration mechanisms, delamination, a separation of concrete layers typically caused by corrosion of steel rebars, is one of the most prevalent and structurally significant. These hidden defects compromise the durability of bridge decks and can progress to spalling and eventual degradation in the structural performance. Since delamination is not visually observable, inspectors have traditionally relied on impact acoustic methods, where variations in sound (such as ringing versus hollow) indicate the presence of defects. Manual sounding techniques, such as hammer tapping and chain dragging, remain widely used by state Departments of Transportation (DOTs) due to their simplicity and low cost.

However, conventional acoustic sounding methods suffer from critical limitations. The process is inherently subjective and depends heavily on an inspector's auditory interpretation and experience. It is also labor-intensive, requiring surface gridding and individual point-wise testing, making it time-consuming, inconsistent, and prone to human error. Environmental noise, variable impact forces, and limited accessibility to vertical or overhead surfaces further reduce the reliability and efficiency of these methods. Uncontrolled broadband impact sounding may fail to capture frequency-specific signatures from defects such as shallow delamination, which often resonate within the 1–3 kHz range.

Despite these challenges, impact-based sounding remains one of the most trusted nondestructive evaluation (NDE) methods for concrete decks in practice. According to a

*Corresponding Authors: Deepak Kumar.
Email: dkumar@ataneconsulting.com
[1]Engineer, ATANE Consulting, New York, NY 10005
[2]Professor of Civil Engineering, The City College of New York, NY 10031
[3]Associate Professor, Hunan University, Hunan, China

Discussion period open till six months from the publication date. Please submit separate discussion for each individual paper. This paper is a part of the Vol. 2 of the International Journal of Bridge Engineering, Management and Research (BER), ISSN 3065-0569.

2024 Federal Highway Administration (FHWA) survey of state highway agencies, methods such as hammer sounding, chain dragging, and impact echo are among the most commonly used and are perceived as reliable for concrete deck evaluation.[2] Fig. 1 shows a comparison of the performance of various methods based on the FHWA study. These findings highlight the continued relevance of traditional acoustic methods while pointing to the need for modernization of the sounding approach to improve its consistency, objectivity, and data capture.

Advances in acoustic sounding and automation

Over the past two decades, researchers have sought to automate and improve acoustic sounding through better hardware and signal processing. Tong et al.[3] and Luk et al.[4,5] applied wavelet transforms and hidden Markov models to impact-acoustic signals for defect detection in bonded structures. Popovics[6] introduced a rolling cart with multiple hammers and microphones that used power spectral density (PSD) analysis to map delamination, though it required the cart to remain stationary during each strike. Sun et al.[7] introduced a continuous scanning device using smooth steel "ball-chain" drags and short-time Fourier transform analysis. This design reduced low-frequency noise (<5 kHz) and increased coverage speed, but it still required contact and was limited to horizontal surfaces. Larsen et al.[8] implemented a multichannel impact mechanism for continuous deck inspection from a moving vehicle, while Hendricks et al.[9] demonstrated high-speed, impact-echo testing for rapid data collection. These systems significantly reduced human involvement, but their mechanical complexity introduced challenges related to weight, power demands, and operational stability. In a more unconventional approach, Blaney and Gupta[10] explored using drones to drop small hammers and record acoustic responses. However, payload limitations and flight stability hindered practical implementation. Despite their promise, fully autonomous mechanical impact systems remain constrained by size, payload, and the need for physical contact at each test point. These limitations restrict deployment on small or airborne robotic platforms and confine inspections to accessible, contact-friendly surfaces.

Noncontact excitation and chirp-based methods

To overcome the contact-related limitations, researchers have explored noncontact acoustic sources. Noncontact NDE techniques aim to excite vibrations in the structure without direct impact, thereby avoiding some constraints of mechanical systems. High-power speakers and even focused electric spark discharges have been studied as impact alternatives that can launch stress waves into concrete from a standoff distance.[11,12] Such approaches can potentially enable fast, continuous scanning since no physical reset is needed between test points. Dabous and Feroz[13] further reviewed the state-of-the-art noncontact testing technologies for condition monitoring of bridges, highlighting the potential for automated data acquisition and processing, an area that Smart Acoustic Sounding System (SASS) directly builds upon. Among these, broadband chirp signals offer significant advantages: they excite a wide range of structural resonant modes in a single sweep, and post-processing

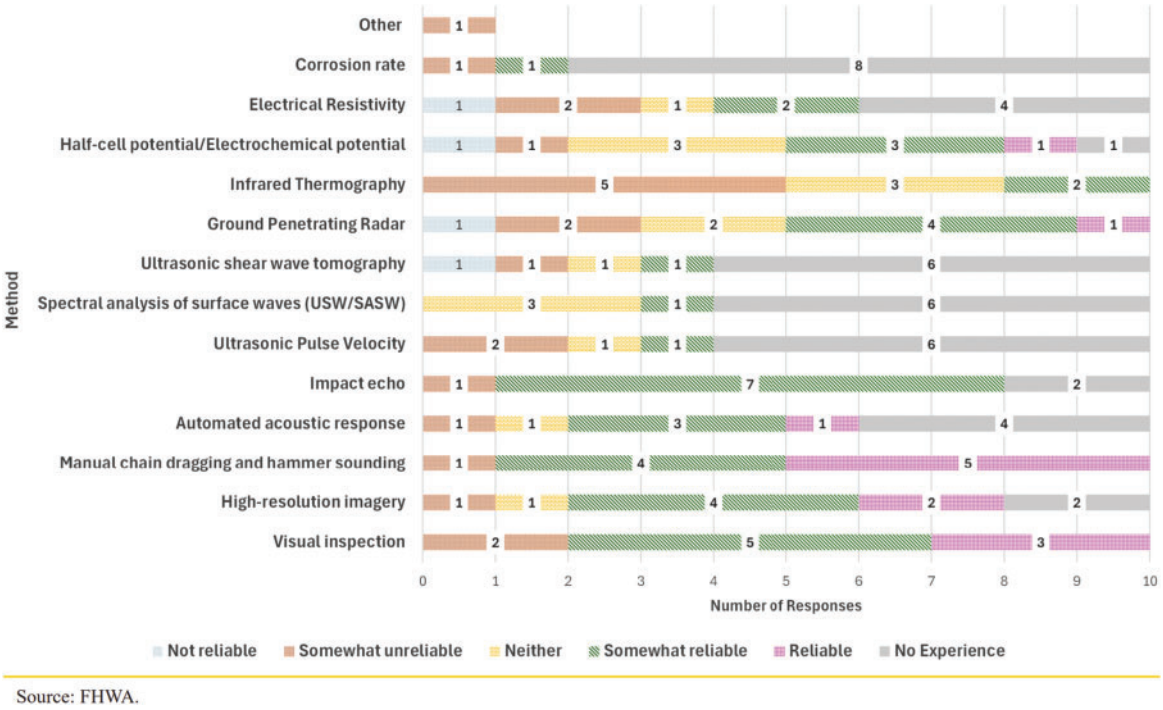

Figure 1. Reported confidence levels of various NDE methods used for concrete bridge deck evaluations, based on FHWA's 2024 survey

allows for targeted frequency-band analysis. Michaels et al.[14] demonstrated the effectiveness of chirp excitation in guided wave testing, showing improved defect imaging through multifrequency excitation. Michaels et al.[15,16] expanded on this by demonstrating how chirp-generated acoustic wavefield images can be used for high-resolution defect visualization, validating the use of chirp excitations in complex structural materials. Similarly, Feng et al.[17] and Mizutani and Inokawa[18] used chirp-excited Lamb waves for delamination detection in composite plates, an approach that translates well to concrete bridge decks. Chirp-based excitation provides standardized, repeatable inputs that are independent of operator variability. It also supports rapid repetition and is well-suited for integration with robotic systems. By covering a wide frequency range, chirp signals can excite multiple resonant modes simultaneously. Preliminary studies suggest that shallow delamination in concrete responds strongly in the 1–3 kHz range, while pristine areas exhibit energy at higher frequencies, an insight that informed the detection algorithms developed in this study.

ML and AI integration

In parallel, machine learning (ML) has emerged as a powerful tool for pattern recognition in acoustic NDE. Muramatsu et al.[19] proposed a noncontact approach for flaw detection using neural network classification of signals from laser Doppler vibrometers, showing the growing influence of artificial intelligence (AI)–driven feature classification in vibration and acoustic analysis. Ye et al.[20] implemented an online learning system where human inspectors' classifications were used to train an algorithm in real time. More recent efforts include the application of deep learning. For example, Alhebrawi et al.[21] used AI to identify concrete cracks from acoustic hammer data with high accuracy. Convolutional neural networks (CNNs), combined with acoustic emission sensors, have shown effectiveness in recognizing time–frequency patterns of crack signals.[22,23] Jafari and Dorafshan[24] applied Naïve Bayes classifiers to features extracted from impact-echo signals, while Barbosh et al.[25] used wavelet-enhanced deep learning for damage localization. Another emerging trend is the integration of multiple NDE modalities with autonomous data collection. Hoxha et al.[26] combined impact-echo and ground-penetrating radar with visual SLAM (Simultaneous Localization and Mapping) for navigation, creating a robotic platform capable of generating three-dimensional defect maps through sensor fusion. Lavadiya and Dorafshan[27] reviewed deep learning applications across NDE domains and emphasized the importance of data consistency and sensor integration. They noted that variability across acquisition systems hampers reproducibility, highlighting the value of standardized excitation and processing. Similarly, Scherr and Grosse[28,29] argued that inconsistent signal quality undermines the comparability of NDE results and advocated for improved data quality control.

This technological convergence of advanced sensing and AI was summarized in our recent review,[30] which outlined the role of hybrid approaches where decomposed acoustic signals (e.g., via empirical mode decomposition [EMD], PSD) are fed into ML models such as CNNs, support vector machines (SVMs), or ensemble classifiers to enhance the detection of delamination, cracking, and other anomalies. However, a significant challenge remains in developing generalizable AI models that can adapt to variable field environments and data sources. Lehman[31] similarly stressed the importance of data-driven inspection tools in national infrastructure assessments.

Gap and study objective

Despite advances in mechanized and AI–driven methods, current approaches to bridge deck inspection continue to face key challenges: heavy reliance on operator skills, the mechanical complexity of contact-based systems, and inconsistent data interpretation across different platforms. To address these limitations, this study introduces a SASS, which is a portable and fully integrated framework that reimagines conventional sounding. SASS incorporates:

- a programmable broadband chirp excitation source for consistent, repeatable impacts,
- Micro-Electro-Mechanical Systems (MEMS) microphones with acoustic shielding for robust noise suppression,
- visual SLAM cameras for location-aware defect mapping, and
- real-time signal processing and ML algorithms (EMD, Hilbert–Huang transform [HHT], PSD) for automated classification.

This system is designed for pole-mountable or portable deployment, enabling reliable inspection of both horizontal and overhead surfaces with minimal human input. Laboratory and field experiments on slabs with artificial defects and deteriorated beams validate its performance.

The key contributions of this work are:

- Development of a standardized, broadband chirp-based sounding method for operator-independent delamination detection.
- Integration of acoustic, visual, and computational modules into a single automated inspection device.
- Demonstration of real-time defect mapping and classification accuracy through laboratory and field experiments.

Methodology

Overview of research approach

This study follows a two-phase experimental approach to develop and validate the SASS. The methodology integrates system development, laboratory testing, and comparative evaluation against conventional manual sounding methods. In the first phase, a large-scale concrete slab embedded with engineered defects, including shallow and deep delamination, honeycomb regions, and voids, was tested

using traditional hammer-based acoustic methods. A handheld hammer was used to apply impacts across the slab surface, and the resulting acoustic signals were recorded and analyzed. This baseline evaluation served to characterize the frequency responses of each defect type while also documenting the challenges of manual inspection, such as subjectivity, inconsistent impact force, and the absence of automated localization. In the second phase, the same specimen was tested using the SASS developed in this study. The system integrates an electronic chirp excitation device, which generates a broadband acoustic pulse in a controlled and repeatable manner. A high-sensitivity MEMS microphone captures the resulting structural response, and a visual SLAM–based tracking camera logs the spatial coordinates of each impact location. This hardware combination enables real-time, location-aware defect mapping without requiring manual surface gridding or positioning.

Signal data collected from both traditional and smart methods were processed using advanced signal processing algorithms. These techniques filter noise, isolate dominant frequency content, and extract relevant features for automated classification. A supervised ML model was then trained to classify each acoustic response based on these features. This two-phase design enabled direct, side-by-side comparison of manual and smart methods under identical conditions, and allowed for assessment of how automation improves repeatability, objectivity, and efficiency in field inspections.

Test specimen and defect configuration

A full-scale concrete slab in the NDE laboratory of the FHWA Turner Fairbank Highway Research Center has been used as a controlled test bed for acoustic sounding experiments. The slab measures 40 inches by 120 inches in plan, with a thickness of 8 inches. Within this slab, four types of artificial defects were embedded during casting to simulate common defects simulating deterioration in bridge decks: a shallow delamination, a honeycomb, a void, and a deep delamination. The delamination defects were simulated using thin plexiglass inserts placed at specific depths below the top surface (approximately 2.5 inches for the shallow delamination and 6 inches for the deep delamination). The honeycomb region was created by deliberate poor consolidation in one area to create air pockets, and the void was simulated by an inflated bladder that was later removed, leaving an air cavity. The locations and sizes of these defects are shown in Fig. 2, along with a schematic of the slab's reinforcement and construction joints. This controlled specimen allows direct comparison of acoustic signals from known defect areas versus solid (intact) concrete areas. Detailed information about the construction of the slab with defects can be found in Lin et al.[32].

To further validate the applicability of the system under more realistic conditions, an additional concrete beam approximately 6 feet in length was evaluated. Unlike the slab, this beam contained unknown, naturally visible deteriorated regions including cracks and spalls. Its surface was divided into a reference grid and was visually inspected to mark damage-prone areas. This secondary test helped assess how well the system generalized to in situ conditions and to defects not explicitly pre-labeled.

Evaluation of traditional acoustic sounding techniques

In the initial testing phase, traditional manual acoustic sounding using a hammer was employed on the slab. The acoustic response at each impact point was recorded using a high-sensitivity MEMS microphone placed near the test location. Different locations on the slab were impacted multiple times to ensure statistical reliability. Impact signals were recorded at a sampling rate of 44.1 kHz over a 1-second window. In an effort to standardize the excitation and improve signal repeatability, additional tests were conducted using a steel ball mounted on a flexible rod. This setup produced consistent, high-energy impacts and allowed for rapid resetting between tests. The steel ball's sharp acoustic

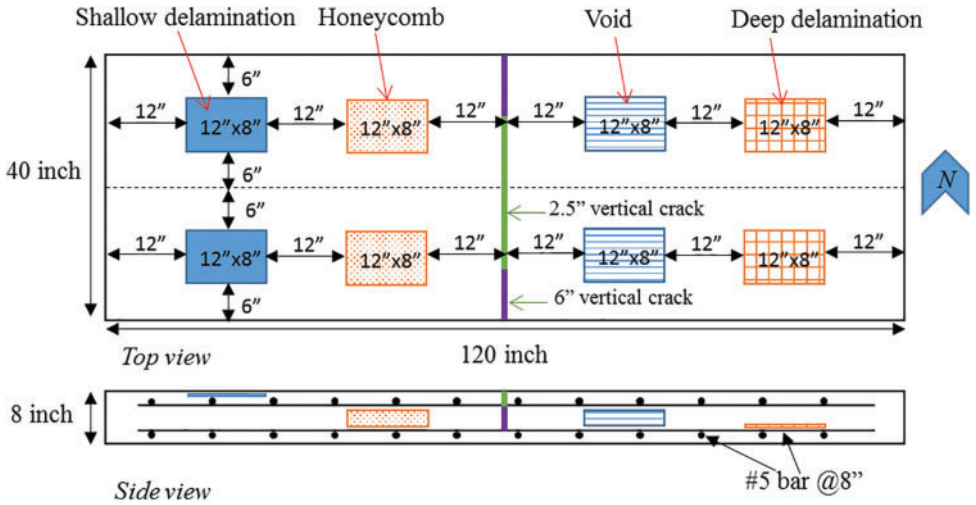

Figure 2. Schematic of the concrete slab specimen with embedded artificial defects, including shallow and deep delamination, honeycombing, and voids

signature and repeatability made it ideal for collecting high-quality reference signals. Across all methods, care was taken to replicate outdoor-like conditions, including the presence of ambient noise and handling variations, to assess signal robustness in practical inspection scenarios.

Signal processing and feature extraction

As data acquisition becomes increasingly automated, the primary challenge in acoustic delamination detection shifts from signal collection to accurate and efficient real-time interpretation. Traditional field methods often rely on auditory cues or basic frequency-domain metrics such as peak frequency. However, these approaches are inherently subjective and highly susceptible to environmental noise and inconsistencies in impact conditions. To overcome these limitations, this study adopted a hybrid signal processing strategy that began with EMD as a front-end noise filter,[33,34] followed by feature extraction using either PSD or Hilbert marginal spectrum (HMS) for frequency-domain analysis, and HHT for energy-based interpretation.

EMD is an adaptive data analysis tool that is commonly used to break down any complicated signal set into several components, which usually pertain to different vibration modes and different physical meanings. These components can also be described as intrinsic mode functions (IMFs), which build a nearly orthogonal basis for the original data

$$y(t) = \sum_{i=1}^{n} x_i(t) + r_n \tag{1}$$

where $y(t)$ is the original signal, $x_i(t)$ is the i_{th} IMF and r_n is the residue.

PSD is a frequency-domain analysis tool that quantifies how the power (energy per unit frequency) of a signal is distributed across different frequencies. It helps identify dominant frequencies and is commonly used in vibration and acoustic analysis. PSD assumes signal stationarity and is calculated as

$$P(f) = \lim_{T\to\infty} |X_T(f)|^2 \tag{2}$$

where $X_T(f)$ is the Fourier transform of the time-limited signal. Although useful for identifying peaks and comparing energy content, PSD does not preserve the time variation of frequency components, which limits its utility in analyzing short, nonstationary signals like impact sounds.

HHT is a two-step method for analysis of nonlinear and nonstationary signals.[35] The first step uses EMD that decomposes the original signal into a finite number of IMFs as shown in Eq. (1). The second step of HHT is the Hilbert transform, which produces an orthogonal pair for each IMF that is phase-shifted by 90°

$$H[x_i(t)] = \frac{1}{\pi}\int_{-\infty}^{\infty} \frac{x_i(\tau)}{t-\tau}\, d\tau \tag{3}$$

The analytic function $A_i(t)$ of any real signal $x(t)$ can be defined as

$$A_i(t) = x_i(t) + jH[x_i(t)] \tag{4}$$

or

$$A_i(t) = a_i(t)\, e^{j\theta_i(t)} \tag{5}$$

where

$$a_i(t) = \sqrt{x_i^2(t) + H^2[x_i(t)]} \tag{6}$$

$$\theta_i(t) = \arctan\frac{H[x_i(t)]}{x_i(t)} \tag{7}$$

The instantaneous frequency can be defined as

$$\omega_i(t) = \frac{d\theta_i(t)}{dt} \tag{8}$$

After performing the Hilbert transformation, the original signal can be obtained from the real part of the analytic function $A_i(t)$. The frequency-time distribution of the amplitude is designated as the Hilbert spectrum $H(\omega, t)$,

$$H(\omega, t) = \mathrm{Re}\left(\sum_{i=1}^{n} a_i(t)\, e^{j\int \omega_i(t)dt}\right) \tag{9}$$

From the Hilbert spectrum, HMS[36] can be defined as

$$H(\omega) = \int_0^T H(\omega, t)\, dt \tag{10}$$

The HMS offers a measure of the amplitude contribution from each frequency over time, while the marginal spectrum provides a measure of the total amplitude (or energy) contribution from each frequency value.

In this study, all acoustic signals recorded by the SASS were first processed using EMD. This adaptive technique separated each raw signal into a finite set of IMFs, each representing local oscillatory behavior. Among these, the first IMF (IMF1) consistently captured the primary transient response triggered by the impact, while the higher-order IMFs typically contained environmental noise, wind-induced vibrations, and mechanical handling artifacts. These noise-dominated IMFs were excluded from further analysis. As a result, EMD functioned as a powerful front-end filter, isolating the most physically meaningful components of the signal prior to spectral interpretation.

With IMF1 extracted, two parallel spectral analysis approaches were applied. First, PSD was computed to quantify how signal energy was distributed across frequencies. This helped identify dominant spectral peaks and allowed for comparative energy-level assessment under different defect conditions. However, PSD assumes stationarity and does not account for time-dependent variations in frequency content. This made it less effective in fully capturing the dynamics of impact-based acoustic signals. To address this limitation, HHT was applied to IMF1, generating the corresponding HMS, which retained the temporal evolution of frequency content while integrating it over time. This provided a more informative view of nonstationary acoustic responses, particularly useful for short-duration events typical of hammer-sounding inspections. Both PSD and HMS revealed distinct frequency bands consistently associated with defect types; for instance, shallow delamination was characterized by elevated energy in the 1.5–3 kHz range. From these processed spectra, a comprehensive set of quantitative features was extracted. These included peak frequency, spectral centroid, mean frequency, and energy content within

predefined diagnostic bands (e.g., 1.5–3, 2–4, and 5–7 kHz). These features were chosen to capture subtle yet consistent spectral differences between sound and defective zones, thereby enhancing the discriminative power of the system.

Although both PSD– and HMS–derived features proved effective in characterizing signal behavior, HMS features consistently provided sharper separation between healthy and defective areas, particularly under noisy or variable field conditions. The combined use of PSD and HMS, both derived from EMD–filtered IMF1, enabled a robust and flexible feature extraction process across varying signal qualities. This integrated framework established a reliable foundation for the subsequent ML–based classification of delamination and other defects.

ML for automated defect classification

A supervised ML approach[37,38] was developed to automatically classify each measurement point as either "defect" or "sound," with the ability to further differentiate specific defect types based on extracted acoustic features. A dataset comprising over 1,100 sample points was compiled from controlled testing on the concrete slab. Each sample corresponded to a known physical location with ground truth labels, such as shallow delamination, deep delamination, honeycomb, void, or intact concrete, and was paired with a set of features extracted from the corresponding acoustic response.

Building on the spectral analysis of signals processed through PSD and the HMS of EMD–filtered IMF1, the features for ML were derived. Several diagnostic frequency ranges were identified: a low-frequency band (~1.5–3 kHz) associated with shallow delamination, a mid-frequency band (~2–4 or 2–5 kHz) often linked with general defect behavior, and higher-frequency bands (5–7 and 6–10 kHz) where intact concrete typically exhibited stronger responses. For each sample, the area under the normalized spectrum within these bands, representing band-limited energy, was computed as input features. Additional features included the dominant frequency, which proved effective in differentiating between sound and defective zones.

Various classification algorithms were tested, including decision trees,[39] SVMs,[40] and ensemble methods.[41] Among these, a decision tree classifier was selected for its strong balance between predictive accuracy and interpretability. The model was trained using 70% of the labeled dataset and evaluated on the remaining 30%. The ML model achieved high accuracy in distinguishing between sound and defective points. Remarkably, the model was also able to identify an unlabeled surface crack on the slab, which was not included in the training dataset. This "unseen" region was correctly flagged as damaged, demonstrating the model's ability to generalize learned patterns beyond explicitly defined categories.

Although more advanced models such as neural networks could be explored in future work, the current dataset size favored simpler classifiers. The decision tree model also offered the advantage of real-time execution on the embedded processor, aligning with the system's design goals of portability and on-device analytics for field deployment.

Design and integration of smart sounding system

Building upon insights from conventional impact testing, a portable SASS was developed to deliver consistent excitation, suppress ambient noise, and automate both data acquisition and defect classification. The system is designed for use on both flat and overhead concrete surfaces, addressing key limitations of traditional methods such as operator subjectivity, inconsistent impact force, and physical fatigue associated with manual chain drag or hammer sounding.

Fig. 3a illustrates the system components and operation. A high-power vibration speaker embedded in a cylindrical acoustic waveguide (approximately 0.5 m in length) functions as the broadband chirp excitation source. When

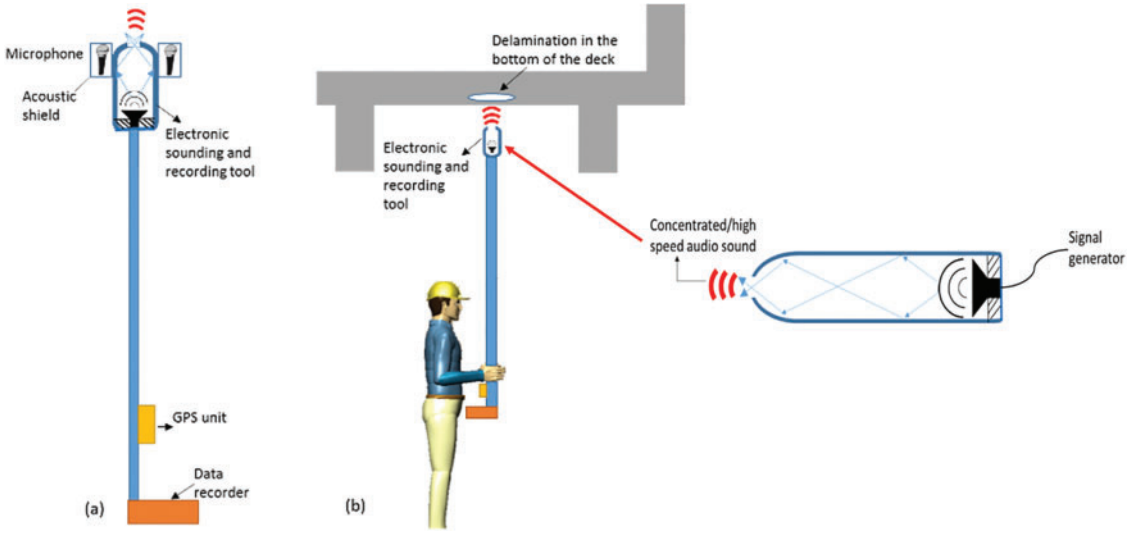

Figure 3. Overview of the Smart Acoustic Sounding System (SASS): (a) system components including chirp speaker, MEMS microphone, and SLAM camera; (b) pole-mounted setup for inspecting overhead concrete surfaces

the tube is pressed against a concrete surface, it concentrates acoustic energy into the material, analogous to a localized shock wave. A programmable signal generator emits chirp signals sweeping from approximately 500 Hz to 16 kHz, covering the key resonance frequencies for typical defects like delamination (~1–3 kHz), while also capturing higher-frequency reflections from intact areas. The chirp signal can be initiated via a graphical user interface or a remote-control interface, ensuring consistency and eliminating manual impacts.

A MEMS microphone, positioned near the tube opening and enclosed within an acoustic shield, records the structural response. Foam gaskets at the rim provide sealed contact, minimizing airborne noise and improving signal-to-noise ratio. A stereovision tracking camera mounted near the device captures the spatial coordinates of each test point using visual SLAM. As the system is swept across a surface, a virtual inspection grid is automatically generated, eliminating the need for manual marking or gridding.

On-board hardware manages signal generation, data acquisition, and real-time processing. Once activated, the system executes the full inspection loop: chirp emission, acoustic response recording, EMD–based signal filtering, spectral feature extraction, defect classification, and real-time visualization of results. This workflow typically completes within a few seconds per test point. The unit is lightweight, battery-powered, and designed for field use. It can be operated by hand or mounted on an extendable pole, as illustrated in Fig. 3b, for testing the undersides of bridge decks or other overhead surfaces. Its integrated processing and sensing capabilities remove the need for external computing tools or surface preparation, enabling rapid and repeatable inspections.

Results and Discussion

Laboratory testing of the developed detection algorithm

To establish baseline performance and identify acoustic signatures for various defect types, laboratory experiments were conducted using manual hammer sounding. The test setup is shown in Fig. 4. A handheld hammer was used to strike the surface of a large concrete slab embedded with engineered defects. A common vocal microphone wrapped with foam to suppress ambient noise was positioned near the impact point to capture the structural acoustic response. The microphone was connected via USB to a laptop for signal acquisition and real-time recording at a sampling rate of 44.1 kHz (Fig. 4a). The basic defect detection mechanism is illustrated in Fig. 4b, where impact-induced stress waves reflect off subsurface anomalies, and the returning signal is recorded for analysis.

Fig. 5 presents the Fourier spectra of acoustic responses from five distinct test locations: a sound area (no delamination), a shallow delamination, a honeycomb region, a void, and a deep delamination. The spectrum corresponding to the intact (sound) area (Fig. 5a) shows distinct high-frequency peaks, primarily above 4 kHz, indicating strong resonant behavior of solid concrete. In contrast, shallow delamination (Fig. 5b) and honeycomb (Fig. 5c) cases exhibit broader, flatter spectra with most energy concentrated below 4 kHz. These low-frequency components are associated with disrupted wave propagation caused by internal defects. The spectrum for the void (Fig. 5d) also displays prominent energy in the low-frequency range, with reduced high-frequency response. Notably, deep delamination (Fig. 5e) shows spectral characteristics more similar to intact concrete than to shallow defects, suggesting that manual sounding may be less sensitive to defects located deep beneath the surface. In all defect cases, multiple low-frequency peaks appear below 2.5 kHz, likely corresponding to flexural modes and environmental or residual noise.

To further isolate and interpret these signals, EMD was applied. The results, shown in Fig. 6, decompose each raw signal into IMFs, enabling adaptive separation of signal and noise content. The original PSD plots (first column) reveal total frequency content. In most cases, the IMF1 (second column) captures the dominant acoustic signal corresponding to the actual impact response. Subsequent IMFs (IMF2 and IMF3) (third and fourth columns) primarily capture low-amplitude noise, confirming the effectiveness of EMD as a noise filtering tool. Across all defect types, the IMF1

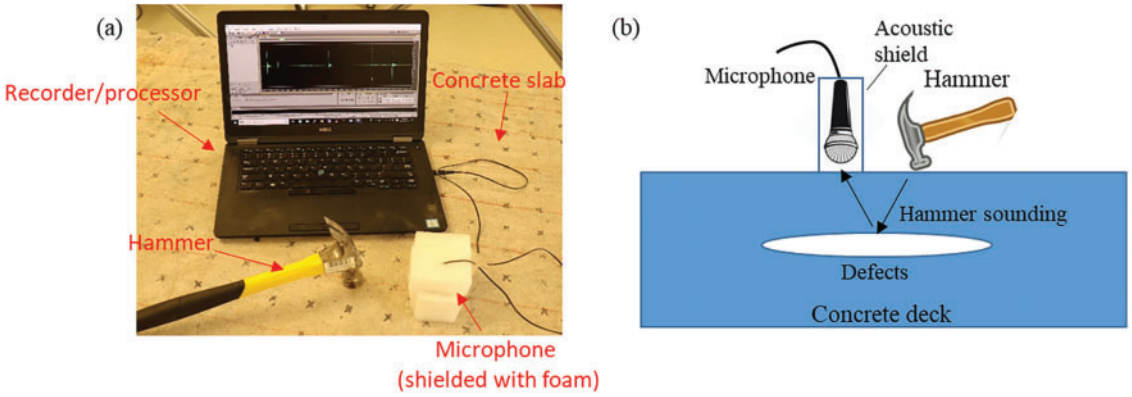

Figure 4. Manual acoustic sounding setup: (a) sounding instruments; (b) conceptual illustration of acoustic wave propagation

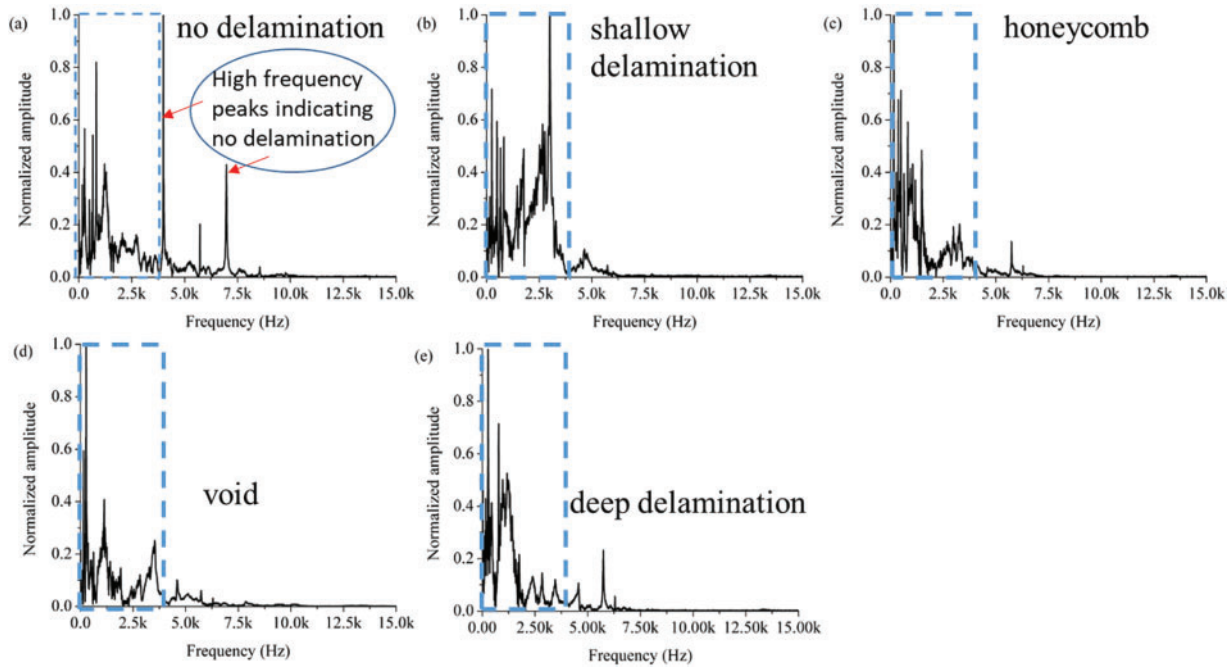

Figure 5. Frequency spectra from hammer sounding at five locations: (a) intact concrete, (b) shallow delamination, (c) honeycomb, (d) void, and (e) deep delamination

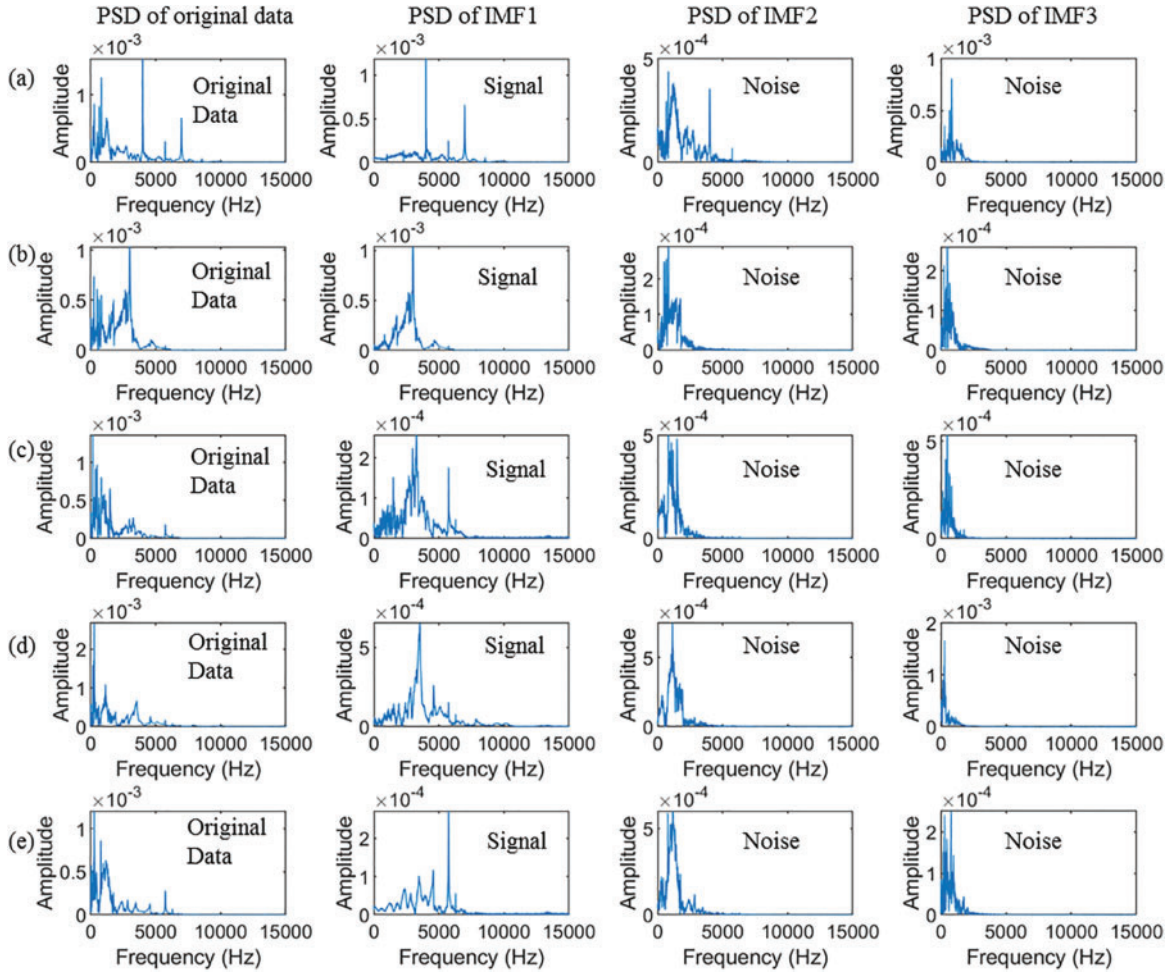

Figure 6. EMD results for hammer sounding signals across five defect conditions: (a) intact, (b) shallow delamination, (c) honeycomb, (d) void, and (e) deep delamination

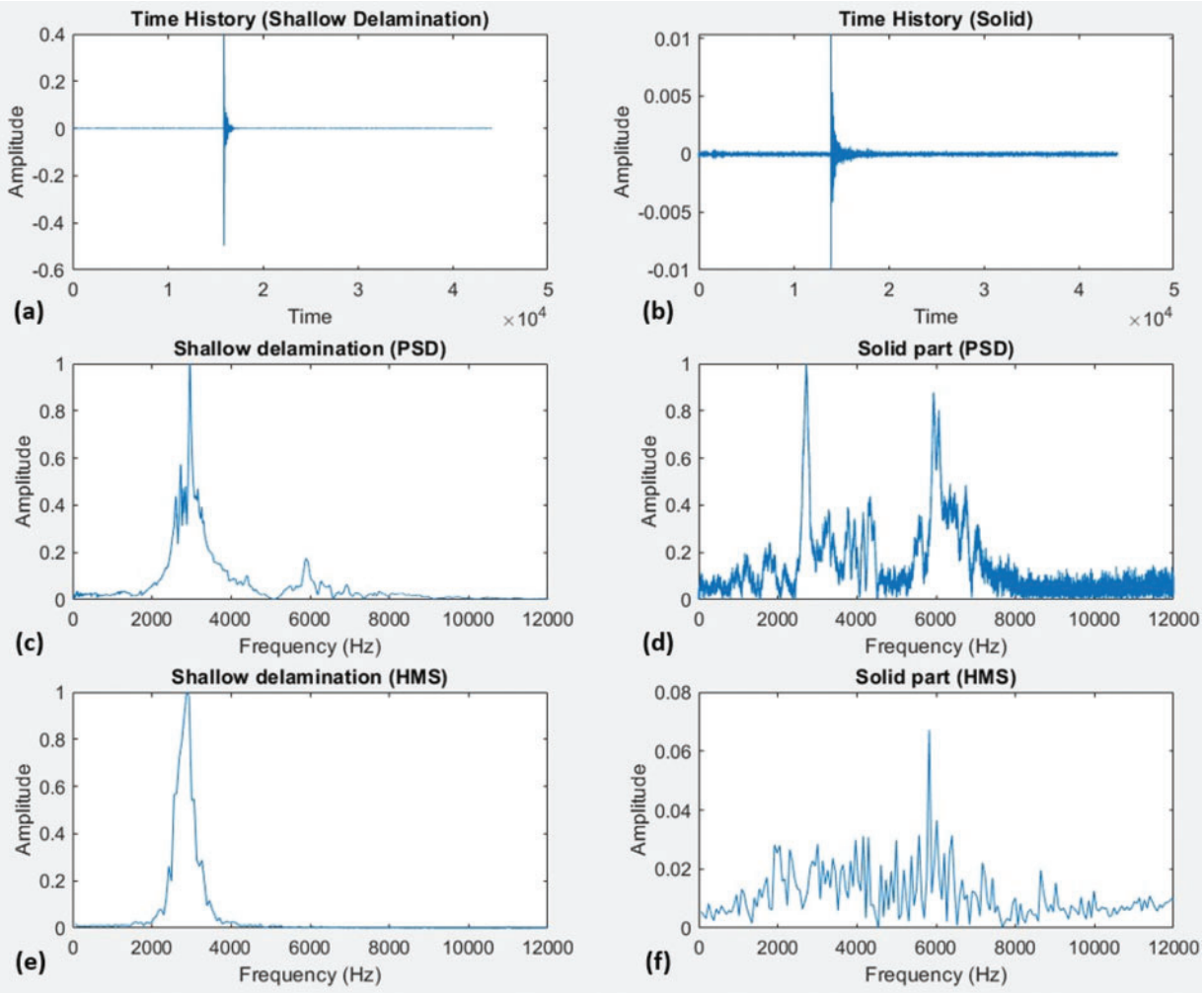

Figure 7. Comparison of time and frequency responses for shallow delamination and solid zones: (a, b) time histories, (c, d) PSD plots, and (e, f) HMS plots

spectra preserve the key low-frequency resonance signatures observed in raw data while suppressing random noise. The differences between defect and sound conditions become more apparent post-EMD, demonstrating how filtering and decomposition enhance interpretability. These processed signals later serve as inputs for feature extraction and ML classification.

The time-history plots of signals for shallow delamination and solid surfaces, shown in Figs. 7a and 7b, respectively, show clear differences between the delaminated and solid areas. The delaminated region has a higher peak and vibrates for a longer time, while the solid area shows a faster decay and lower amplitude. After applying EMD, the IMF1 was used to calculate both the PSD and the HMS (Figs. 7c–7f). These plots highlight important differences: the delamination case shows stronger energy in the lower frequency range (1.5–3 kHz), while the solid region spreads energy across higher frequencies above 3 kHz. In particular, the HMS plot for the solid part shows more scattered and weaker low-frequency energy. These results support using a frequency threshold and ML for accurate defect classification.

Frequency-based damage index visualization using PSD and HMS

To enhance the detection and spatial visualization of subsurface defects, a damage index metric was developed based on frequency-domain analysis. This index is defined as the ratio of spectral energy in the 2–4 kHz band to the total energy in the 0–8 kHz range and was computed using both the PSD and HMS of IMF1 signals. The 2–4 kHz frequency range was chosen based on prior observations indicating that shallow delamination consistently exhibits dominant energy in this band.

Fig. 8a presents the layout of the concrete slab used in this study, showing the locations of engineered defects, including shallow delamination, honeycomb, void, and deep delamination, as well as two surface cracks that occurred naturally during curing. At each grid point, a hammer was used to excite the slab, and the acoustic response was recorded using a foam-shielded microphone. The recorded signals were decomposed using EMD to isolate the dominant response (IMF1), from which spectral features were extracted for index calculation. The resulting PSD–based damage index map is shown in Fig. 8b. Ground-truth defect locations

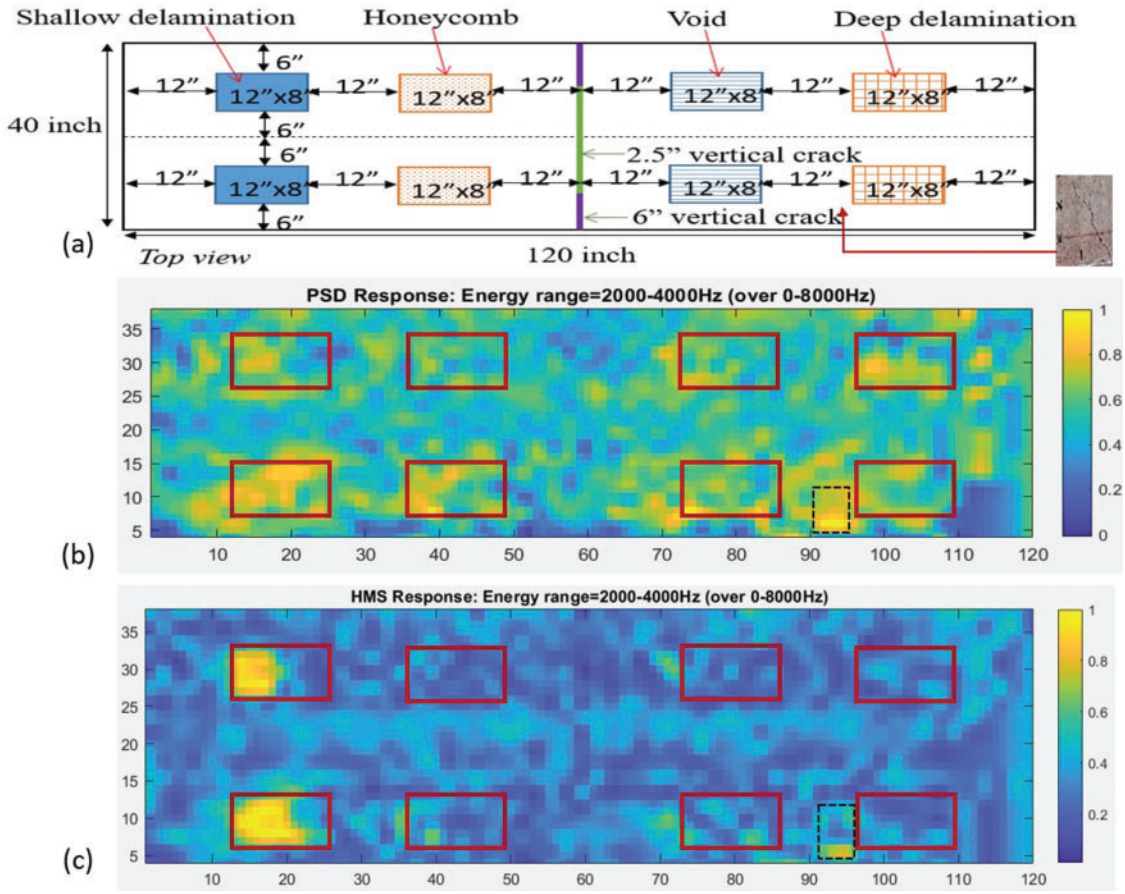

Figure 8. (a) Defect layout of the concrete slab, (b) damage map visualization using PSD, and (c) damage map using HMS

are marked with red rectangles. The PSD plot effectively highlights several damage zones, particularly the shallow delamination areas and a horizontal crack near the lower right region, which appears as a bright patch. However, the deep delamination region is less distinguishable, consistent with earlier findings that hammer sounding is relatively less effective in detecting deeper defects. Fig. 8c shows the HMS–based damage index map, which leverages time-integrated energy from the nonstationary acoustic signal. The shallow delamination zones appear more localized and better defined in the HMS plot compared to the PSD results. Additionally, the background (non-defect) regions show reduced noise and higher contrast, enhancing defect visibility. However, HMS displays reduced sensitivity to voids and deep delamination, as expected from its frequency-energy focus.

In summary, while both PSD and HMS provide valuable insights into damage localization, HMS offers enhanced clarity and spatial contrast for detecting shallow delamination, often the most critical for early maintenance intervention. PSD, on the other hand, is more responsive to broader spectral anomalies such as cracks and voids. Together, these complementary techniques support improved diagnosis of surface-level and subsurface deterioration, with HMS being especially useful for identifying early-stage, non-visible damage.

ML–based defect detection algorithm

While earlier studies[42,43] often relied on a single frequency band, typically 1.5–3 kHz, to identify damaged regions in concrete structures, this approach has limitations due to its subjectivity and narrow scope. Although this frequency range has shown utility in identifying shallow delamination, the effectiveness of such fixed-band approaches can vary depending on the defect type and surrounding material conditions. In response to this limitation, the present study introduces an ML framework that leverages multiple diagnostic frequency bands and statistical signal features to automatically classify defects with higher robustness and generalizability.

To train and validate the ML model, a dataset of more than 1100 acoustic response points was collected from a controlled concrete slab at the FHWA Resource Center. The slab measured 40 inches by 120 inches and included various engineered defects such as shallow delamination, honeycombs, voids, and deep delamination. Acoustic signals were acquired every two inches across the grid, ensuring dense spatial coverage. Each recorded data point was paired with a ground-truth label corresponding to its physical condition. The acoustic responses were preprocessed using EMD, and features were extracted from the IMF1 to ensure noise-filtered spectral data.

Instead of selecting a single spectral band, the ML model utilized multiple frequency-based features, including the area under the normalized spectral curve across several bands such as 1.5–3, 2–4, 2.5–4, 5–7, and 6–10 kHz. Additional time-domain statistics, such as signal mean and variance, were also computed. These features enabled the model to learn characteristic patterns associated with both sound and defective zones. A decision tree classifier was chosen for its balance of accuracy and interpretability, and was trained using 70% of the dataset, with the remaining 30% used for validation.

The classifier achieved high accuracy in identifying damaged zones across the slab. As shown in Fig. 9, the predicted damage regions (highlighted in yellow) align closely with the actual defect zones marked by red dashed boxes. Importantly, the model also detected an unlabeled vertical surface crack at the center of the slab, demonstrating its ability to generalize beyond the training data. This finding highlights the model's strength in learning structural damage patterns and applying them to novel conditions.

The successful detection of both known and unknown defect areas underscores the potential of supervised ML models in acoustic-based NDE. Unlike fixed-band techniques, the data-driven approach captures subtle differences in signal characteristics across a range of frequencies. This approach, thus, allows for more nuanced and accurate classification of various defect types, including those not explicitly represented during training. The ability to operate in real-time on embedded processors further supports the field deployment of such models as part of portable inspection systems.

Chirp-based excitation and signal processing for automated defect detection

The use of chirp-based excitation represents a significant advancement over traditional hammer sounding for concrete inspection. The experimental setup shown in Fig. 10 demonstrates a portable electronic configuration, where a vibration speaker generates a chirp signal directed at the concrete surface, and the resulting acoustic response is captured using a foam-shielded microphone. Compared to manual impact methods, this approach offers repeatability, reduced operator dependency, and the potential for robotic deployment. The chirp signal, spanning 0–10 kHz, can be triggered repeatedly without variation in amplitude, allowing for controlled, high-resolution frequency analysis.

Fig. 11 presents the source chirp and the corresponding recorded response, with the latter showing the system's sensitivity to subsurface conditions. By applying cross-correlation

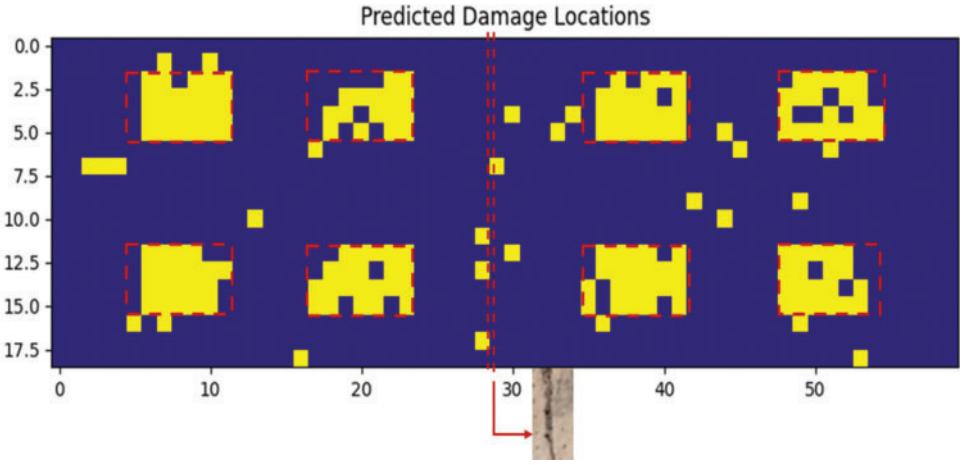

Figure 9. Machine learning–based defect prediction map from hammer acoustic data

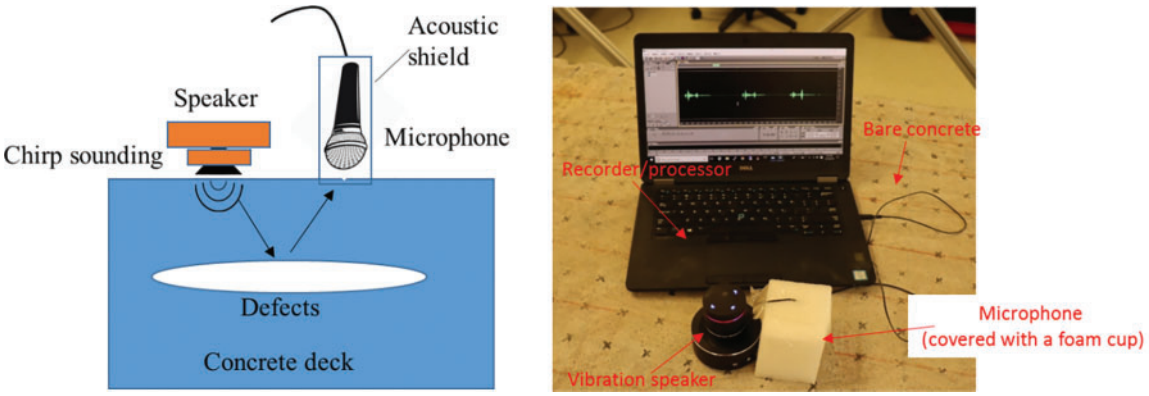

Figure 10. Chirp excitation test setup: (a) SASS components during slab testing and (b) schematic of acoustic signal emission and response capture

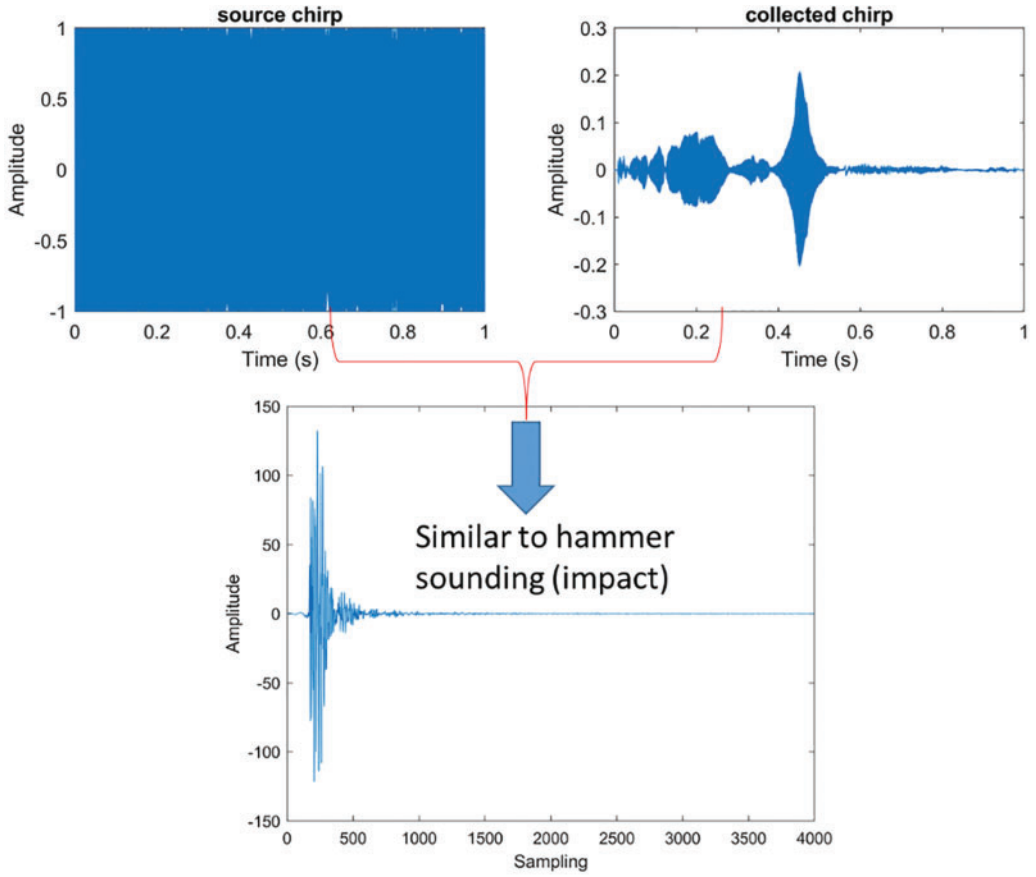

Figure 11. Illustration of cross-correlation of chirp sounding data

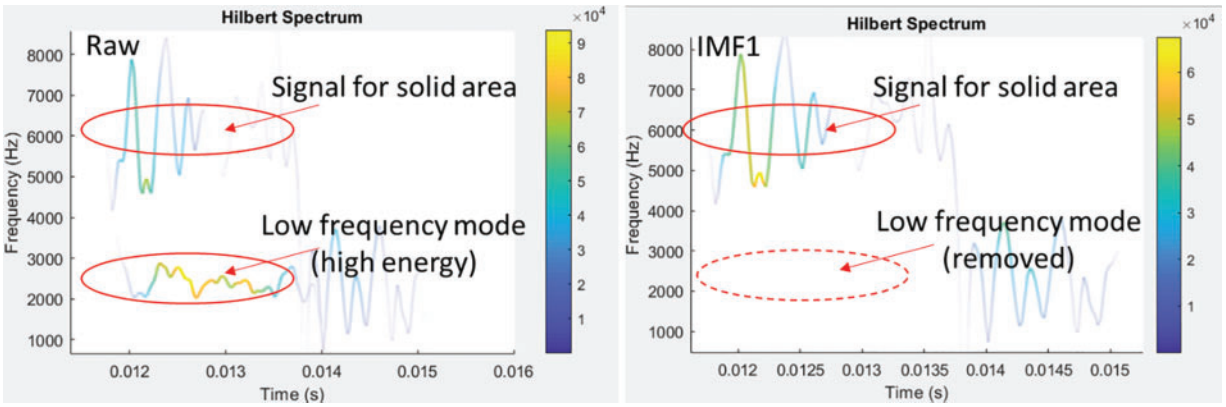

Figure 12. Noise suppression in chirp data using empirical mode Decomposition (EMD)

between the transmitted and received chirp signals, phase variations were removed, enhancing the signal-to-noise ratio. Notably, the resulting waveform closely resembles that of hammer sounding but exhibits much less ambient noise.

To further isolate structural responses, EMD was applied to the correlated chirp signal, followed by HHT analysis. As depicted in Figs. 12 and 13, the EMD method effectively removed low-frequency noise, with IMF1 containing most of the signal energy related to structural vibrations. The HHT spectrum of the filtered data (Fig. 13) revealed dominant frequencies in the 6–7 kHz range for solid regions and 2–3 kHz for delaminated areas, consistent with earlier hammer-based findings.

Fig. 13 confirms that EMD-filtered chirp responses are comparable in behavior to hammer sounding while offering higher repeatability and reduced noise interference. These insights validate chirp excitation as a reliable alternative for detecting shallow delamination, with EMD and HHT providing robust signal filtering and time-frequency resolution. This combined methodology enhances the detection capability of the smart sounding system and paves the way for automated, scalable NDE solutions for bridge decks and concrete structures.

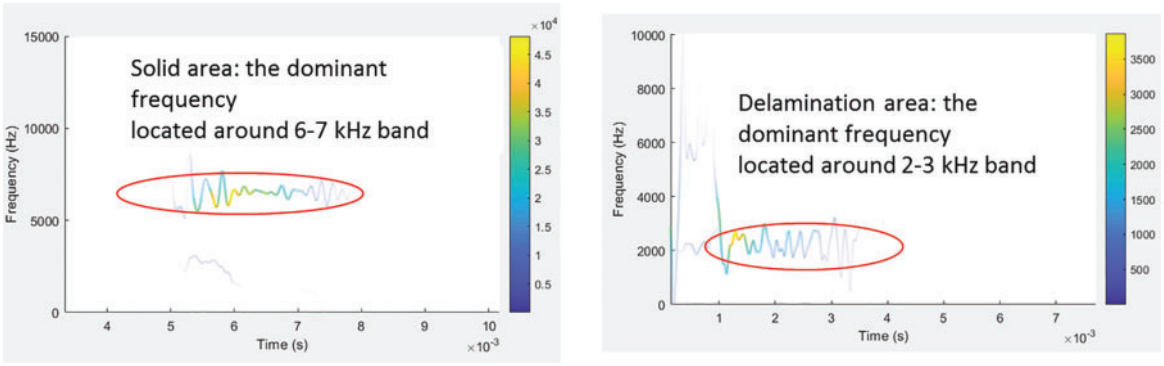

Figure 13. HHT spectrum showing instantaneous energy distribution from the EMD-filtered chirp signal for solid and delamination areas

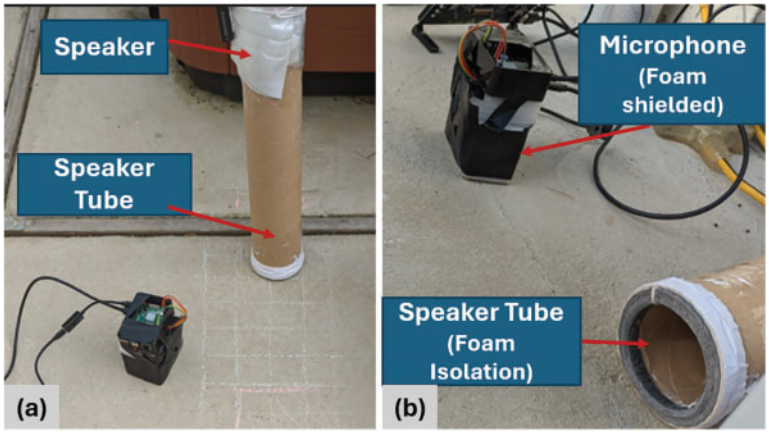

Figure 14. (a) SASS testing on concrete slab and (b) foam insulation ring added to reduce acoustic leakage from speaker tube

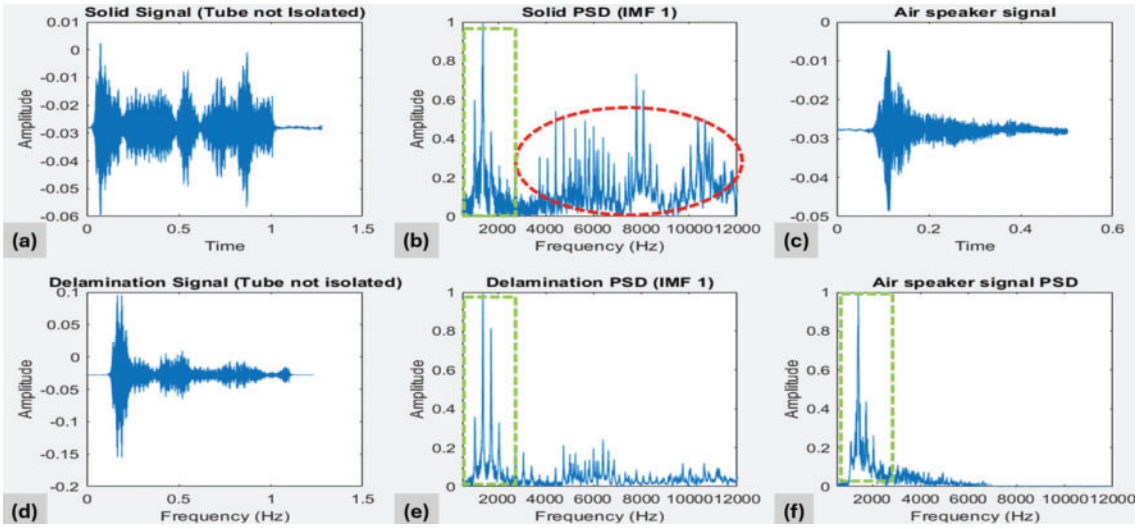

Figure 15. Effect of speaker isolation on acoustic signals: (a, c, d) time-domain responses and (b, e, f) PSD–based frequency spectra for solid and defective conditions

Smart sounding tool evaluation

Controlled experiments were conducted to evaluate the performance of the proposed SASS under both laboratory and field conditions. The testing involved two scenarios: (1) a concrete slab embedded with engineered defects and (2) a deteriorated in situ concrete beam located in an existing building. These scenarios allowed assessment of system behavior in both controlled and practical environments.

Fig. 14 shows the test setup on the concrete slab. Initial testing of the concrete slab showed that solid

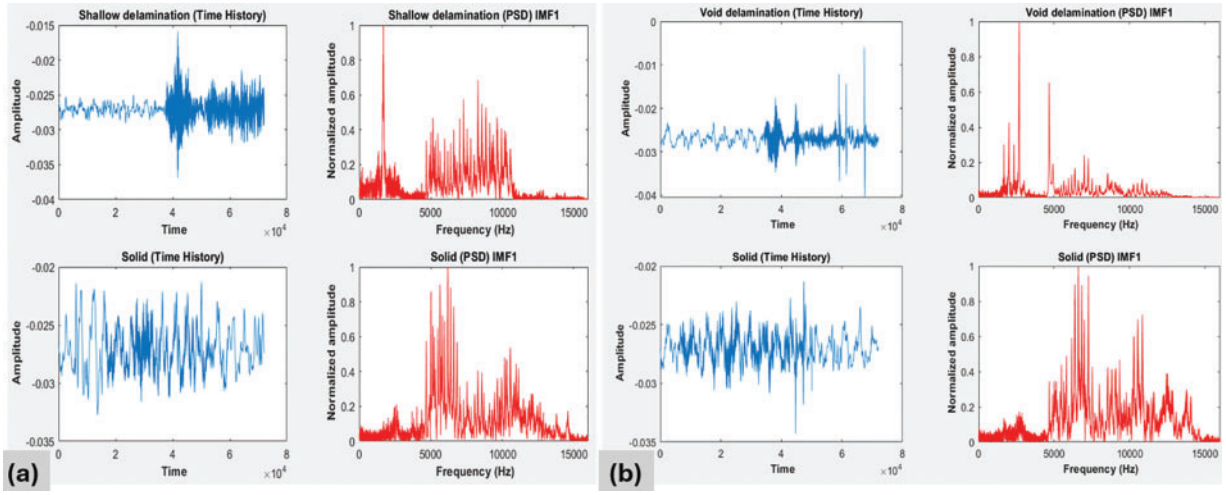

Figure 16. Frequency-based comparison of shallow and void delamination signals versus solid regions using PSD

Figure 17. Deteriorated concrete beam at CCNY campus

regions generated higher excitation beyond 3 kHz, corroborating past research findings. However, inconsistencies were observed in the lower frequency domain. Unexpectedly, defective areas did not exhibit significantly stronger responses at frequencies below 3 kHz, and instead, showed a similar spectral profile to the solid zones. Upon further investigation, it was determined that acoustic leakage from the speaker, due to inadequate sealing between the speaker tube and the rough concrete surface, was contaminating the signal. The sound, bypassing the concrete, directly reached the microphone, resulting in misleading low-frequency components in the PSD. Fig. 15 illustrates this issue, showing that the airborne noise emitted by the speaker dominates the frequencies below the 3 kHz region, masking the surface vibrations critical for defect detection.

To mitigate this interference, a circular foam ring was installed at the base of the speaker tube to ensure tighter acoustic isolation between the speaker and the concrete surface (see Fig. 14b). This modification significantly reduced noise intrusion and allowed for more accurate measurement of surface-transmitted signals. With the enhanced setup, subsequent testing produced results that aligned closely with theoretical and empirical expectations. As shown in Fig. 16, shallow delamination and voids now exhibited prominent spectral peaks below 3 kHz, while solid regions maintained dominant responses above this threshold. This clear separation validated the application of a 3 kHz threshold as a reliable criterion for distinguishing defective zones from intact concrete.

Field testing on a damaged beam

The refined system was field-tested on a deteriorated concrete beam as shown in Fig. 17. A grid pattern of 6 × 6-inch squares (Fig. 19) was used for mapping, and signals were collected at each node using the smart sounding tool. The frequency-domain response from each grid cell was analyzed by integrating spectral energy in the 1.5–3 kHz band, a frequency range previously associated with shallow defects.

The PSD and HMS outputs from EMD–filtered IMF1 signals revealed strong correspondence between low-frequency excitation and known damaged areas (Fig. 20). Delaminated zones showed elevated spectral energy within the 1.5–3 kHz range, while solid areas showed dominant responses above this range. HMS plots provided complementary visual evidence of energy concentration in defect-prone locations.

The smart sounding system accurately identified damaged regions, which were visually represented using a color-coded grid in Fig. 19. Purple zones corresponded to visibly damaged regions such as delamination, cracks, and spalling (e.g., grids 4, 9, 14, and 32), while yellow indicated moderate or potential damage. Interestingly, some surface-visible cracks (e.g., grid 6) were not flagged as defects, likely due to intact bonding behind the surface, highlighting the system's sensitivity to unbonded or hollow regions rather than superficial cracking. Proper microphone-speaker isolation proved essential. Initial tests suffered from airborne speaker noise leakage, which was resolved by the foam ring (Fig. 18), yielding significantly cleaner signals and more

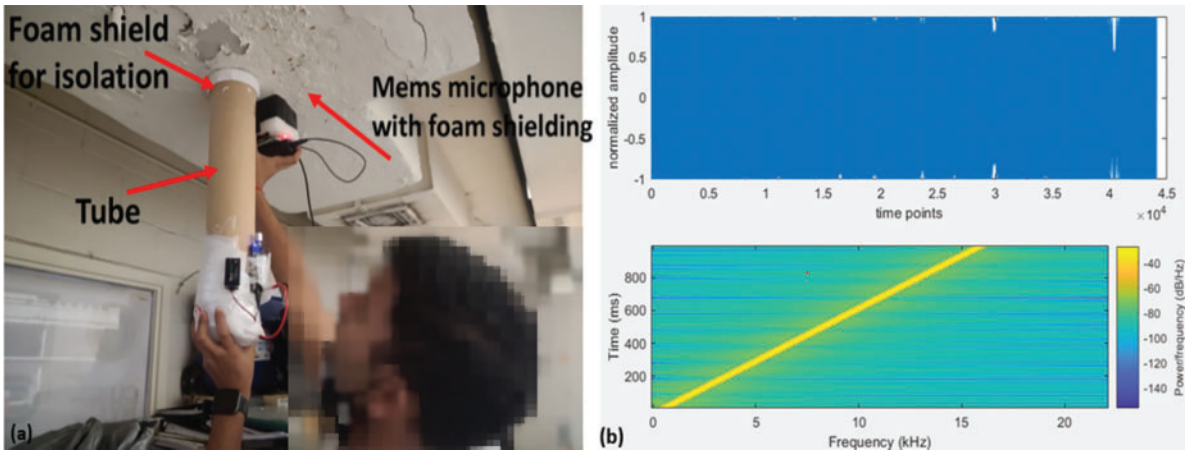

Figure 18. (a) SASS field testing on damaged beam and (b) chirp excitation characteristics used for signal analysis

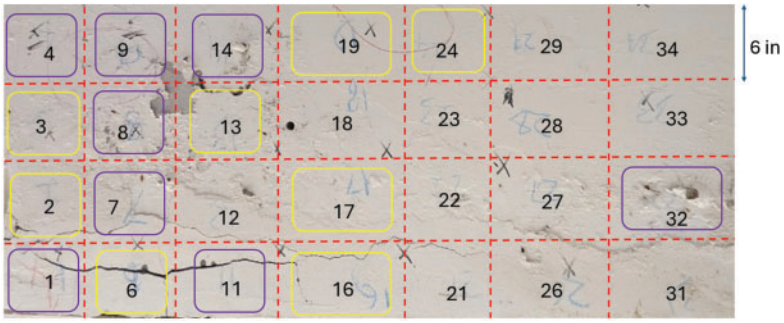

Figure 19. Defect mapping of deteriorated concrete beam using color-coded grid overlay with chirp-based acoustic data

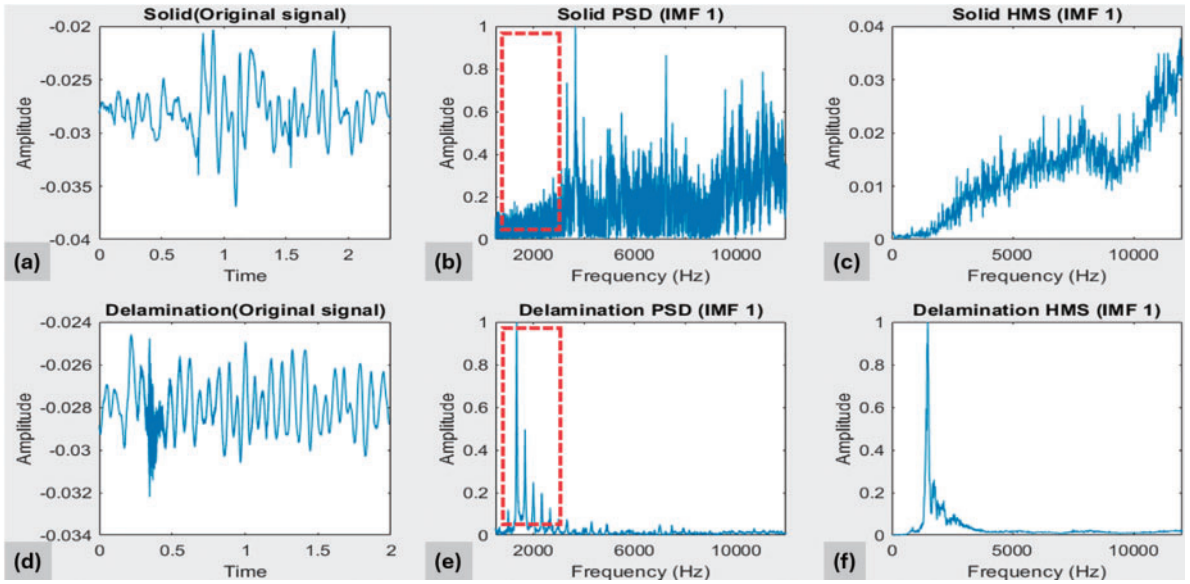

Figure 20. Time and frequency responses for solid and delaminated zones: (a, d) time-domain signals, (b, e) PSD plots, and (c, f) HMS plots after EMD filtering

accurate damage differentiation. Overall, the system provided rapid, repeatable, and visually interpretable feedback on shallow defect conditions. Future improvements, such as slimmer tubes, directional speakers, or higher-resolution microphones, could enhance detection depth and resolution, particularly in complex structural settings.

Discussion of novelty and contributions

The SASS developed in this study represents a notable departure from traditional manual impact sounding techniques by addressing key challenges of subjectivity, repeatability, and data interpretation. A primary innovation lies in the use of a programmable chirp signal, which allows consistent

excitation across all test points without dependence on operator skill or variability in force application. This uniformity is crucial for reliable comparison across large surfaces and under varying field conditions.

The integration of EMD and HHT enables the decomposition of noisy, nonstationary acoustic signals into intrinsic components, isolating frequency bands linked to common defects like delamination and voids. HMS analysis, derived from these IMFs, proved superior to conventional PSD in distinguishing closely spaced spectral features. In particular, defect zones showed elevated responses in the 1.5–3 kHz range, which were accurately captured using IMF1–based transformations. The enhanced resolution provided by HMS improved both interpretability and ML model classification performance. The visual SLAM camera further contributes to operational efficiency by automating spatial referencing, allowing direct mapping of test points and defect regions without manual gridding or drawing overlays. This spatial automation supports real-time mapping of deterioration and lays the foundation for digital asset management and robotic inspections.

However, limitations remain. The system currently depends on surface contact through a foam interface, which may limit usage in inaccessible or irregular geometries. Detection is primarily sensitive to near-surface flaws, and expanding its applicability to deeper defects would require broader frequency excitation or alternative techniques such as impact-echo. Field deployment also demands improved environmental shielding and robustness of the electronic components to handle temperature, dust, and moisture variability.

Conclusions

This research demonstrates the feasibility and effectiveness of a SASS for detecting and mapping subsurface defects in concrete. The combination of broadband chirp excitation, EMD–HHT–based signal analysis, and automated spatial tracking enables a portable, objective, and high-resolution inspection method. Controlled laboratory experiments and field validation in an existing building confirmed the system's ability to distinguish solid and defective regions based on frequency-domain features, particularly those in the lower-frequency range associated with delamination. ML classifiers trained on HMS features achieved high accuracy, even generalizing to untrained defect types, demonstrating the robustness of the spectral signatures. The system eliminates many of the manual steps involved in traditional acoustic inspections, such as grid layout, subjective sound interpretation, and post-processing, offering a scalable solution for large-scale bridge assessments. The ability to map results in real-time supports timely maintenance decisions and improved record-keeping for long-term monitoring.

Future work will focus on expanding the training dataset, integrating more advanced classification models, and miniaturizing hardware components to facilitate deployment in constrained environments. Enhancements to system durability and automation will be essential for widespread adoption by transportation agencies and infrastructure managers.

Acknowledgments

This research was conducted as part of the INSPIRE University Transportation Center (UTC) project on autonomous bridge inspection. The authors gratefully acknowledge the funding support from the U.S. Department of Transportation, Office of the Assistant Secretary for Research and Technology (USDOT/OST-R) under Grant No. 69A3551747126 through INSPIRE University Transportation Center (http://inspire-utc.mst.edu) at Missouri University of Science and Technology. We also acknowledge a partial support through a grant from the Social and Economic Mobility for People And Communities through Transportation (SEMPACT) University Transportation Research Center (UTRC), which is the designated United State Department of Transportation UTC for the federal region 2 and is housed at the City College of New York.

Disclaimer

The views, opinions, findings, and conclusions expressed in this paper are solely those of the authors and do not represent the official policy or position of the USDOT/OST-R or any state or other entity.

References

[1] American Society of Civil Engineers. Bridges: 2025 Infrastructure Report Card; 2025. https://infrastructurereportcard.org/cat-item/bridges-infrastructure/.

[2] Federal Highway Administration. *Incorporating Nondestructive Evaluation Methods Into Bridge Deck Preservation Strategies (FHWA-HRT-24-186)*. Washington, DC, United States: Department of Transportation, Federal Highway Administration, Office of Research, Development, and Technology; 2024. doi:10.21949/1521525.

[3] Tong F, XU XM, Luk BL, Liu KP. Evaluation of tile–wall bonding integrity based on impact acoustics and support vector machine. *Sens Actuat A: Phys*. 2008;144(1):97–104. doi:10.1016/j.sna.2008.01.020.

[4] Luk BL, Liu K, Tong F, Man K. Impact-acoustics inspection of tile-wall bonding integrity via wavelet transform and hidden Markov models. *J Sound Vib*. 2010;329(10):1954–1967.

[5] Luk B, Liu K, Tong F. Rapid evaluation of tile-wall bonding integrity using multiple-head impact acoustic method. *NDT & E Int*. 44(3):297–304.

[6] Popovics JS. *Investigation of a Full Lane Acoustic Scanning Method for Bridge Deck Nondestructive Evaluation*. Washington, D.C: Transportation Research Board, Final Report for Highway IDEA Project 134, Transportation Research Board; 2010.

[7] Sun H, Zhu J, Ham S. Automated acoustic scanning system for delamination detection in concrete bridge decks. *J Bridge Eng*. 2018;23(6):04018027.

[8] Larsen JL, McElderry J, Baxter JS, Guthrie WS, Mazzeo BA. Automated sounding for concrete bridge

deck inspection through a multi-channel, continuously moving platform. *NDT & E Int*. 2020;109(32):102177. doi:10.1016/j.ndteint.2019.102177.

[9] Hendricks LJ, Baxter JS, Chou Y, Thomas M, Boekweg E, Guthrie WS, Mazzeo BA. High-speed acoustic impact-echo sounding of concrete bridge decks. *J Nondestruct Eval*. 2020;39:1–12.

[10] Blaney S, Gupta R. Unmanned aerial vehicle-based sounding of subsurface concrete defects. *J Acoust Soc Am*. 2018;144(3):1190–1197.

[11] Akamatsu R, Sugimoto T, Utagawa N, Katakura K. Proposal of non contact inspection method for concrete structures using high-power directional sound source and scanning laser Doppler vibrometer. *Jpn J Appl Phys*. 2013;52(7S):07HC12.

[12] Dai X, Zhu J, Haberman MR. A focused electric spark source for non-contact stress wave excitation in solids. *J Acoust Soc Am*. 2013;134(6):EL513–EL519.

[13] Dabous SA, Feroz S. Condition monitoring of bridges with non-contact testing technologies. *Autom Constr*. 2020;116:103224.

[14] Michaels JE, Lee SJ, Hall JS, Michaels TE. Multi-mode and multi-frequency guided wave imaging via chirp excitations. In: *Proceedings, Health Monitoring of Structural and Biological Systems, International Society for Optics and Photonics*; 2011; San Diego, CA, United States. pp. 79840I.

[15] Michaels TE, Michaels JE, Lee SJ, Chen X. Chirp generated acoustic wavefield images. *Proceedings, Health Monitoring of Structural and Biological Systems, International Society for Optics and Photonics*; 2011; San Diego, CA, United States. pp. 79840I.

[16] Michaels JE, Lee SJ, Croxford AJ, Wilcox PD. Chirp excitation of ultrasonic guided waves. *Ultrasonics*. 2013;53(1):265–270.

[17] Feng B, Ribeiro AL, Ramos HG. A new method to detect delamination in composites using chirp-excited Lamb wave and wavelet analysis. *NDT & E Int*. 2018;100:64–73.

[18] Mizutani Y, Inokawa S. A fundamental study of an inspection method for thin-walled structures using lamb waves induced by chirp signals. *Proceedings, Third International Conference on Experimental Mechanics and Third Conference of the Asian Committee on Experimental Mechanics, International Society for Optics and Photonics*; 2005; Singapore. pp. 520–528.

[19] Muramatsu M, Uchida S, Takahashi Y. Noncontact detection of concrete flaws by neural network classification of laser doppler vibrometer signals. *Eng Res Express*. 2020;2(2):025017.

[20] Ye J, Kobayashi T, Iwata M, Tsuda H, Murakawa M. Computerized hammer sounding interpretation for concrete assessment with online machine learning. *Sensors*. 2018;18(3):833.

[21] Alhebrawi MN, Huang H, Wu Z. Artificial intelligence enhanced automatic identification for concrete cracks using acoustic impact hammer testing. *J Civil Struct Health Monit*. 2023;13(2):469–484. doi:10.1007/s13349-022-00651-8.

[22] Vy V, Lee Y, Yoon H. Crack detection of concrete structures using acoustic emission sensors and convolutional neural networks. In: *The International Conference on Sustainable Civil Engineering and Architecture*. Singapore: Springer Nature Singapore; Jul 2023:1306–1314.

[23] Habib MA, Hasan MJ, Kim JM. A lightweight deep learning-based approach for concrete crack characterization using acoustic emission signals. *IEEE Access*. 2021;9:104029–104050.

[24] Jafari F, Dorafshan S. Bridge inspection and defect recognition with using impact echo data, probability, and Naive Bayes classifiers. *Infrastructures*. 2021;6(9):132. doi:10.3390/infrastructures6090132.

[25] Barbosh M, Dunphy K, Sadhu A. Acoustic emission-based damage localization using wavelet-assisted deep learning. *J Infrastruct Preserv Resil*. 2022;3(1):6. doi:10.1186/s43065-022-00051-8.

[26] Hoxha E, Feng J, Sanakov D, Xiao J. *Robotic Inspection and Subsurface Defect Mapping Using Impact-Echo and Ground Penetrating Radar*. IEEE Robotics and Automation Letters; 2023.

[27] Lavadiya DN, Dorafshan S. Deep learning models for analysis of non-destructive evaluation data to evaluate reinforced concrete bridge decks: a survey. *Eng Rep*. 2023. doi: 10.1002/eng2.12608.

[28] Scherr JF, Grosse CU. Delamination detection on a concrete bridge deck using impact echo scanning. *Struct Concr*. 2021;22(2):806–812.

[29] Scherr JF, Grosse CU, Popovics JS. Evaluation of non-destructive impact-echo data from the national bridge inventory. *Dev Built Environ*. 2024;18:100468.

[30] Kumar D, Agrawal A. Advancing bridge infrastructure management through artificial intelligence: a comprehensive review. *Int J Bridge Eng, Manag Res*. 2025;2(3):214250021–1:18. doi:10.70465/ber.v2i3.45.

[31] Lehman M. The American Society of Civil Engineers' report card on America's infrastructure. In: *Women in Infrastructure*. Cham: Springer International Publishing; 2022:5–21. doi:10.1007/978-3-030-92821-6_2

[32] Lin S, Meng D, Choi H, Shams S, Azari H. Laboratory assessment of nine methods for nondestructive evaluation of concrete bridge decks with overlays. *Constr Build Mater*. 2018;188:966–982.

[33] Cao R, Agrawal AK. Defect detection of concrete structures through sounding data analytics. In: *Proceedings of the 9th International Conference on Structural Health Monitoring of Intelligent Infrastructure*; August 4–7, 2019; St. Louis, MO, USA: ISHMII.

[34] Zhang M, Zhang Q, Li J, Xu J, Zheng J. Classification of acoustic emission signals in wood damage and fracture process based on empirical mode decomposition, discrete wavelet transform methods, and selected features. *J Wood Sci*. 2021;67(1):1–13. doi:10.1186/s10086-021-01990-8.

[35] Huang NE, Wu Z. A review on Hilbert-Huang transform: method and its applications to geophysical studies. *Rev Geophys*. 2008;46(2):RG2006. doi:10.1029/2007RG000228

[36] Li H, Zhang Y, Zheng H. Hilbert-Huang transform and marginal spectrum for detection and diagnosis of localized defects in roller bearings. *J Mech Sci Technol*. 2009;23(2):291–301. doi:10.1007/s12206-008-1110-5.

[37] Nasteski V. An overview of the supervised machine learning methods. *Horizons. b*. 2017;4(51–62):56.

[38] Kotsiantis SB, Zaharakis I, Pintelas P. Supervised machine learning: a review of classification techniques. *Emerg Artif Intell Appl Comput Eng*. 2007;160(1):3–24.

[39] Charbuty B, Abdulazeez A. Classification based on decision tree algorithm for machine learning. *J Appl Sci Technol Trends*. 2021;2(01):20–28.

[40] Suthaharan S. Support vector machine. In: *Machine Learning Models and Algorithms for Big Data Classification: Thinking with Examples for Effective Learning*. Boston, MA: Springer US; 2023:207–235.

[41] Dietterich TG. Ensemble methods in machine learning. In: *International Workshop on Multiple Classifier Systems*. Berlin, Heidelberg: Springer Berlin Heidelberg; June 2023:1–15. doi:10.1007/3-540-45014-9_1

[42] Kumar D, Agrawal AK, Cao R, Zhan L, Wei J. Damage detection in concrete slab using smart sounding. In: Rizzo P, Milazzo A. (Eds.), *European Workshop on Structural Health Monitoring. EWSHM 2022. Lecture Notes in Civil Engineering*. vol. 254. Cham: Springer; 2023. doi:10.1007/978-3-031-07258-1_11

[43] Agrawal AK. *Quantitative Bridge Inspection Ratings using Autonomous Robotic Systems. Project IM-2. 1*. Rolla, Missouri, USA: Missouri University of Science and Technology; 2022. https://scholarsmine.mst.edu/project_im-2/1.